

## Supporting information

# Layer-dependent Electronic and Optical Properties in Tin Monoxide: Potential Candidate in Photovoltaic Application

Li Wanzhong<sup>a\*</sup>, Sun Jian<sup>b\*</sup>, Deng Chong<sup>a</sup>

<sup>a</sup>School of Mechanical Engineering, Xi'an Shiyou University, Xi'an, Shaanxi Province, 710065, P. R. China

<sup>b</sup>School of Mechanical and Electrical Engineering, Xi'an Polytechnic University, Xi'an, Shaanxi Province, 710048, P. R. China

Corresponding Authors: \* E-mail: [liwanzhong@xsyu.edu.cn](mailto:liwanzhong@xsyu.edu.cn) (W. L.)

## Computational Details

The Helmholtz free energy is defined as:

$$F = -\kappa_B T \ln Z$$

with  $k_B$  being the Boltzmann constant and  $T$  the temperature.  $Z$  defines the partitioning of energy among the energy levels associated with the degrees of freedom of the system:

$$Z = \exp(-\varphi / \kappa_B T) \prod_{qv} \frac{\exp(-\hbar\omega(qv) / 2\kappa_B T)}{1 - \exp(-\hbar\omega(qv) / \kappa_B T)}$$

where  $\varphi$  is the potential energy of the system, and the product runs over vibrational modes  $v$  and reciprocal-space wave vectors  $q$ , with the phonon occupation number for each mode obtained from a Bose-Einstein distribution using the characteristic oscillator frequency  $\omega$ .

The temperature-dependent Helmholtz free energy is hence given by:

$$F = \varphi + \frac{1}{2} \sum_{qv} \hbar\omega(qv) + \kappa_B T \sum_{qv} \ln[1 - \exp(-\hbar\omega(qv) / \kappa_B T)]$$

where  $\hbar$  is the reduced Planck constant. The second term is a sum of the modal contributions to the zero-point vibrational energy, and the third term is the contribution of each mode to the free energy due to thermal occupation of the phonon energy levels.

Table S1 The calculated Raman active modes of monolayer, bilayer, and trilayer SnO for the  $\Gamma$  point.

Monolayer	Bilayer	Trilayer
A1 <sub>g</sub> (-0.004)	E <sub>g</sub> (-0.003)	E <sub>g</sub> (-0.002)
E <sub>g</sub> (0.002)	A1 <sub>g</sub> (-0.003)	A1 <sub>g</sub> (-0.001)
E <sub>g</sub> (3.133)	E <sub>g</sub> (0.935)	E <sub>g</sub> (0.678)
A1 <sub>g</sub> (6.016)	A1 <sub>g</sub> (1.091)	A1 <sub>g</sub> (0.812)
E <sub>g</sub> (7.354)	E <sub>g</sub> (3.159)	E <sub>g</sub> (1.161)
B1 <sub>g</sub> (9.845)	E <sub>g</sub> (3.211)	A1 <sub>g</sub> (1.390)
E <sub>g</sub> (12.813)	A1 <sub>g</sub> (5.987)	E <sub>g</sub> (3.163)
A1 <sub>g</sub> (14.975)	A1 <sub>g</sub> (6.111)	E <sub>g</sub> (3.184)
	E <sub>g</sub> (7.560)	E <sub>g</sub> (3.250)
	E <sub>g</sub> (7.637)	A1 <sub>g</sub> (5.945)
	B1 <sub>g</sub> (9.842)	A1 <sub>g</sub> (6.039)
	B1 <sub>g</sub> (9.943)	A1 <sub>g</sub> (6.123)
	E <sub>g</sub> (12.971)	E <sub>g</sub> (7.552)
	E <sub>g</sub> (13.187)	E <sub>g</sub> (7.573)
	A1 <sub>g</sub> (14.766)	E <sub>g</sub> (7.739)
	A1 <sub>g</sub> (15.116)	B1 <sub>g</sub> (9.866)
		B1 <sub>g</sub> (9.919)
		B1 <sub>g</sub> (10.024)
		E <sub>g</sub> (12.941)
		E <sub>g</sub> (13.040)
		E <sub>g</sub> (13.277)
		A1 <sub>g</sub> (14.555)
		A1 <sub>g</sub> (15.037)
		A1 <sub>g</sub> (15.081)

Table S2 The possible reaction paths for SnO and the calculated corresponding reaction enthalpy.

Reaction	$\Delta H$ (eV)
$2\text{SnO} \rightarrow 2\text{Sn} + \text{O}_2$ (1)	6.44
$2\text{SnO} + \text{O}_2 \rightarrow 2\text{SnO}_2$ (2)	-5.28

Table S3 Calculated bandgaps (in eV) for bulk, monolayer, and multilayer SnO using the PBE and HSE06 schemes; effective masses ( $m_e$ ) for hole and electron for bulk, monolayer, and multilayer SnO.

System	PBE	HSE06	Effective mass (electron)			Effective mass (hole)		
			$\Gamma$	X	Z	$\Gamma$	X	Z
Bulk	0.10	0.61	0.42	0.22	0.41	5.91	1.31	0.93
Mono-SnO	3.02	4.05	0.88	1.53		4.21	2.54	
Bi-SnO	1.14	1.81	0.51	0.37		1.72	0.80	
Tri-SnO	0.62	1.20	0.47	0.31		2.94	0.89	
Four-SnO	0.43	0.98	0.46	0.27		3.57	1.06	
Five-SnO	0.28	0.81	0.45	0.24		3.57	1.22	
Six-SnO	0.23	0.74	0.45	0.23		4.17	1.22	
Seven-SnO	0.19	0.71	0.45	0.22		6.25	1.28	

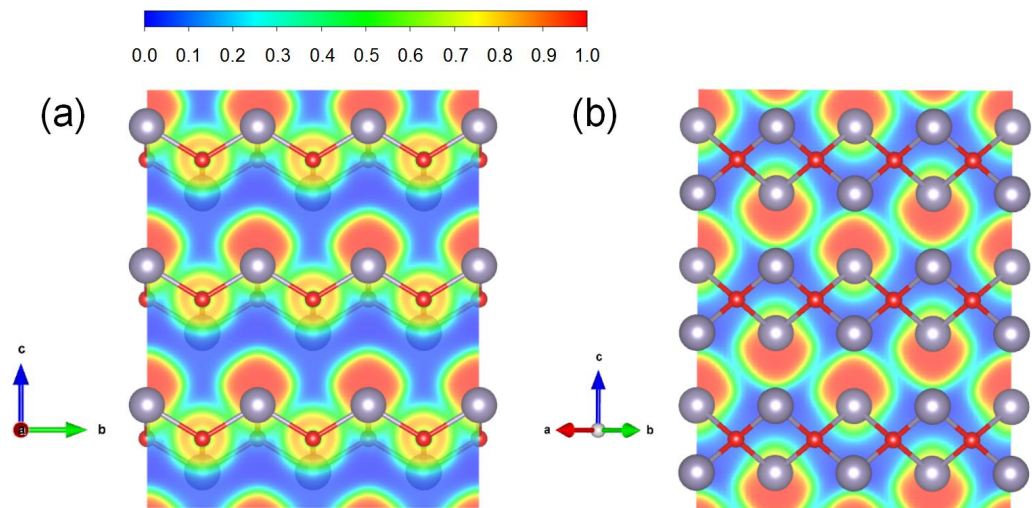


Fig. S1 Electron localization function (ELF) of (a) intralayer Sn-O interactions and (b) interlayer Sn-Sn interactions in bulk SnO.

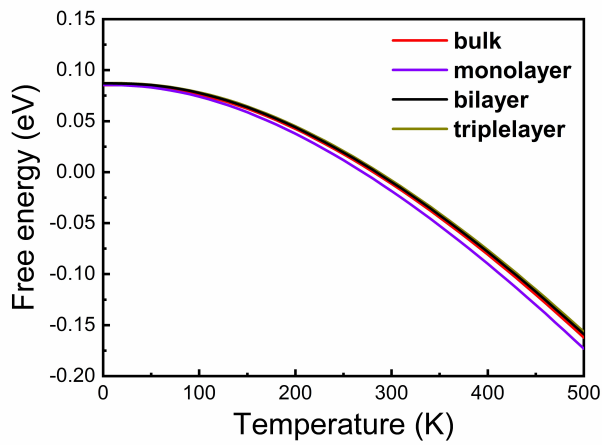


Fig. S2 Temperature-dependent Helmholtz free energy over 0-500 K.

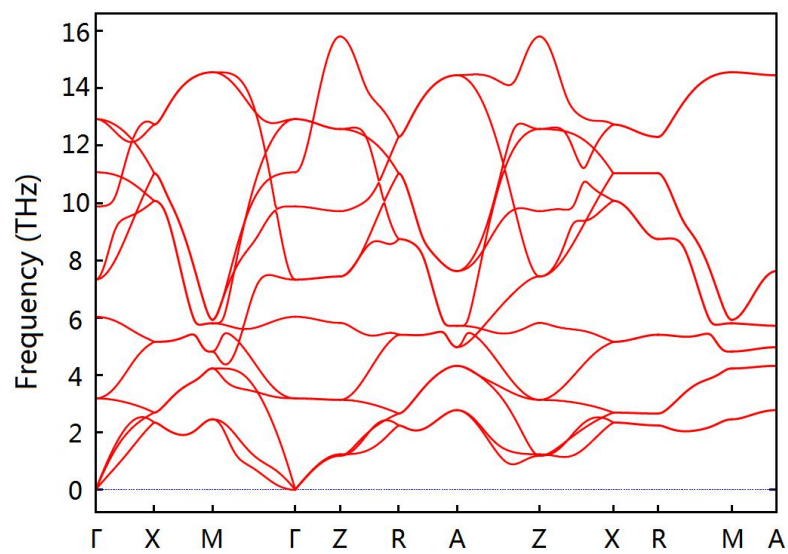


Fig. S3 Phonon dispersion of bulk SnO.

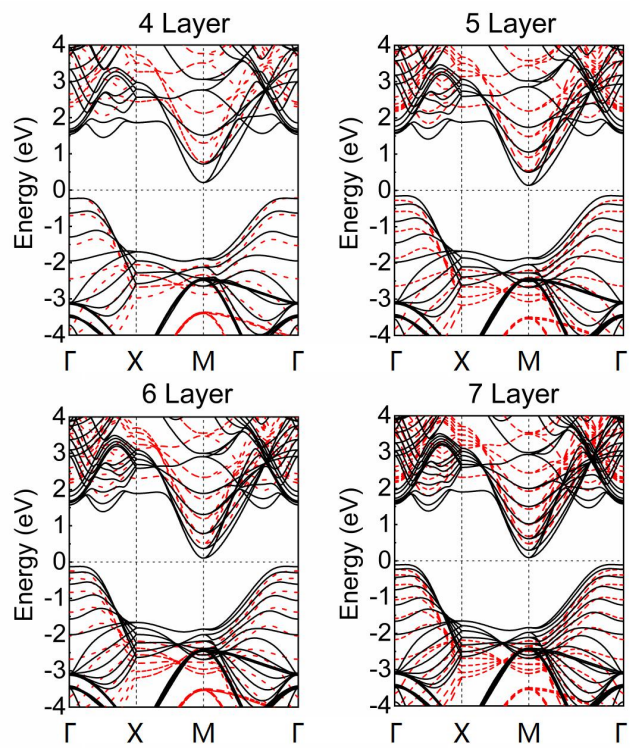


Fig. S4 Band structures for (a) four-layer SnO, (b) five-layer SnO, (c) six-layer SnO, and (d) seven-layer SnO.

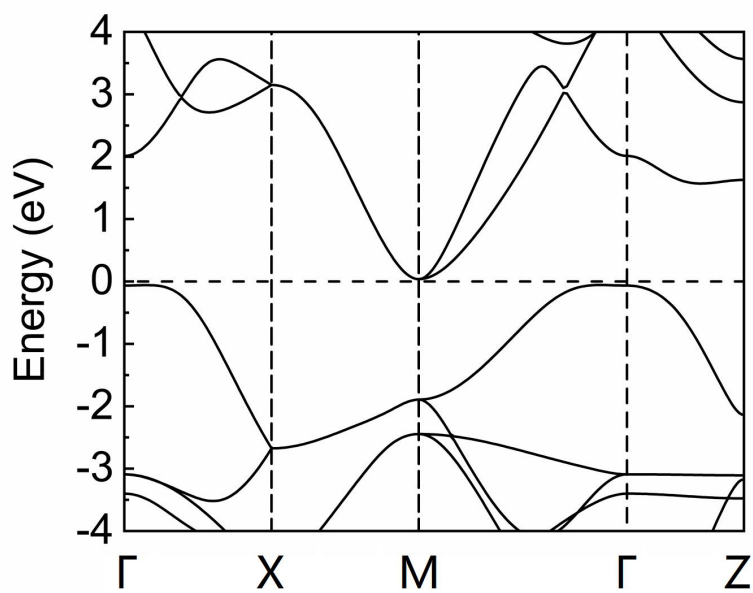


Fig. S5 Band structure of bulk SnO including high symmetry path along the stacking direction  $\Gamma$ -Z.

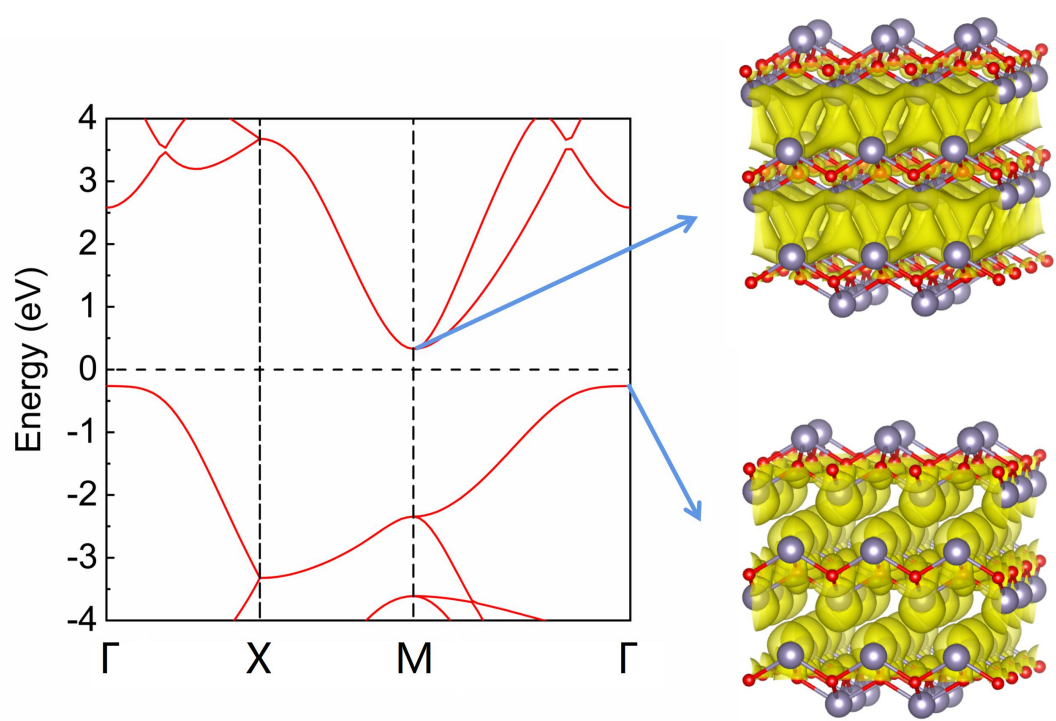


Fig. S6 Band-decomposed charge density of VBE and CBE in bulk SnO.

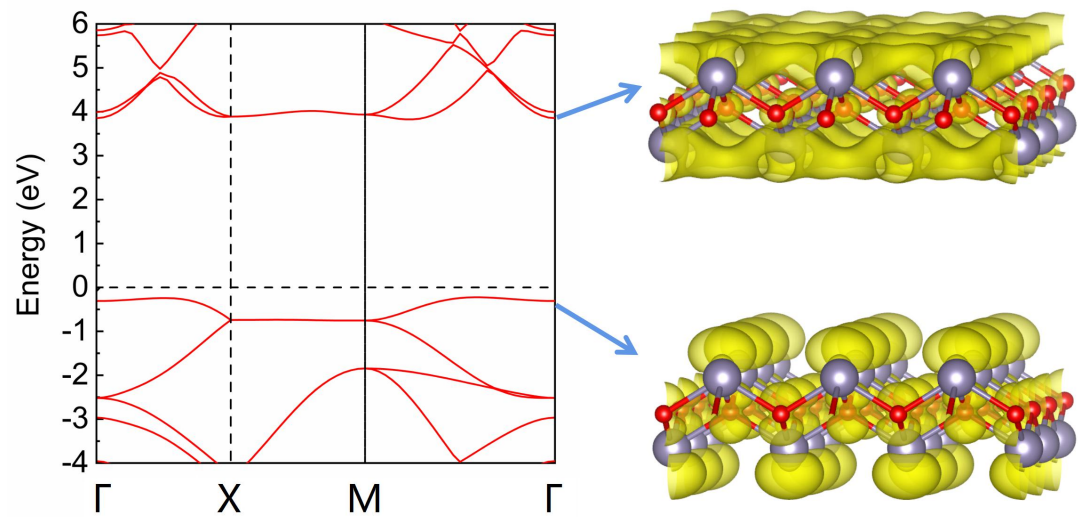


Fig. S7 Band-decomposed charge density of VBE and CBE in monolayer SnO.

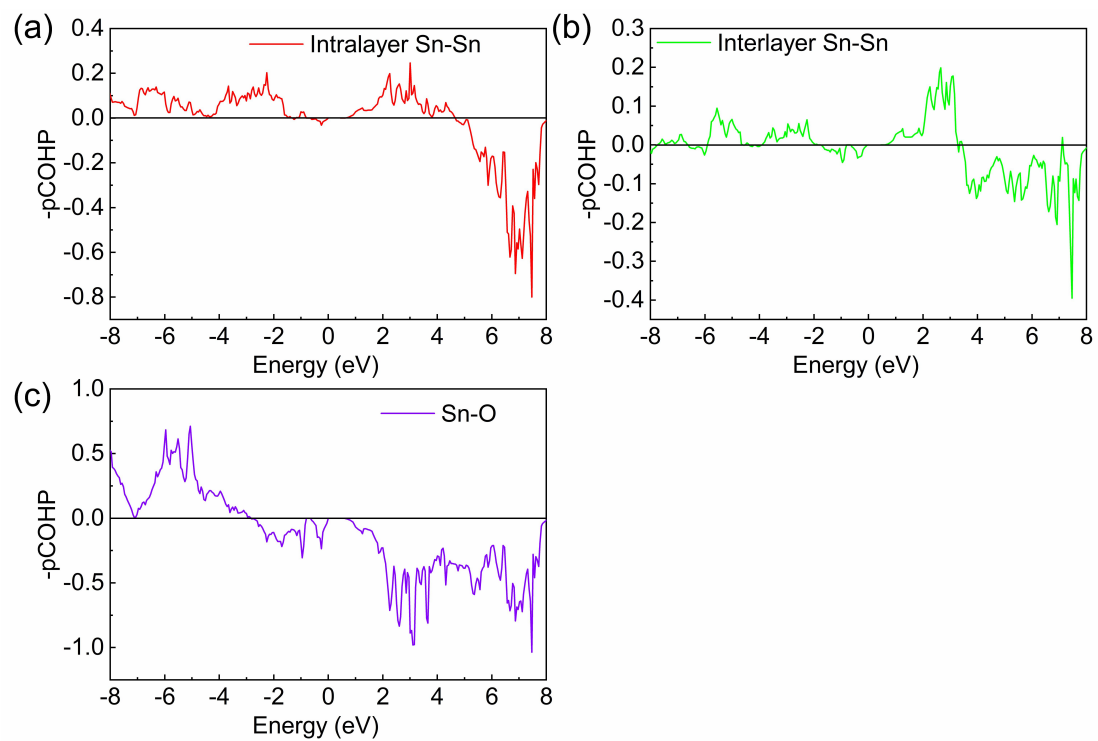


Fig. S8 Crystal orbital Hamiltonian populations for (a) intralayer Sn-Sn interaction, (b) interlayer Sn-Sn interaction, and (c) Sn-O (intralayer) in bulk SnO.

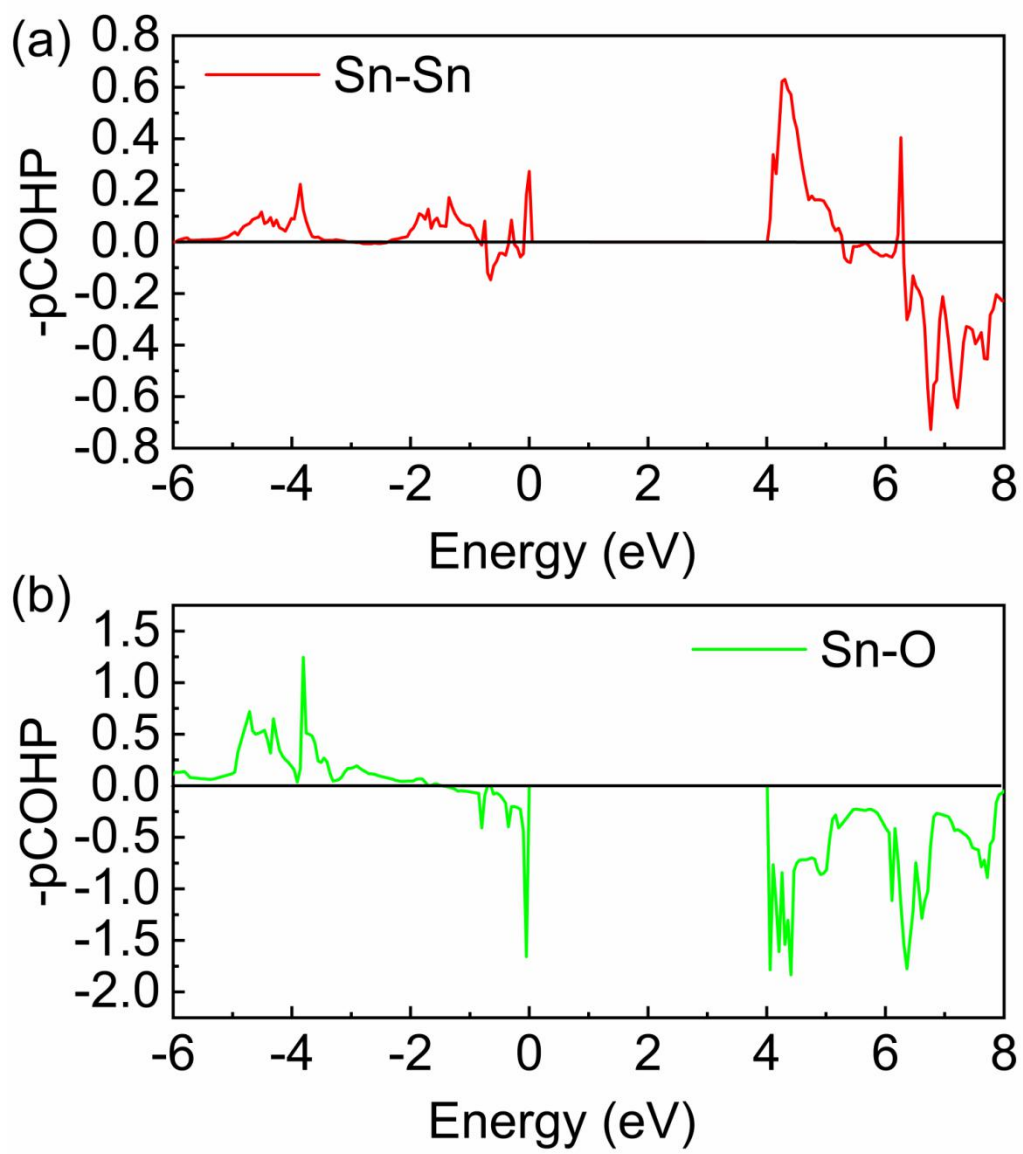


Fig. S9 Crystal orbital Hamiltonian populations for (a) intralayer Sn-Sn interaction, and (b) Sn-O in monolayer SnO.

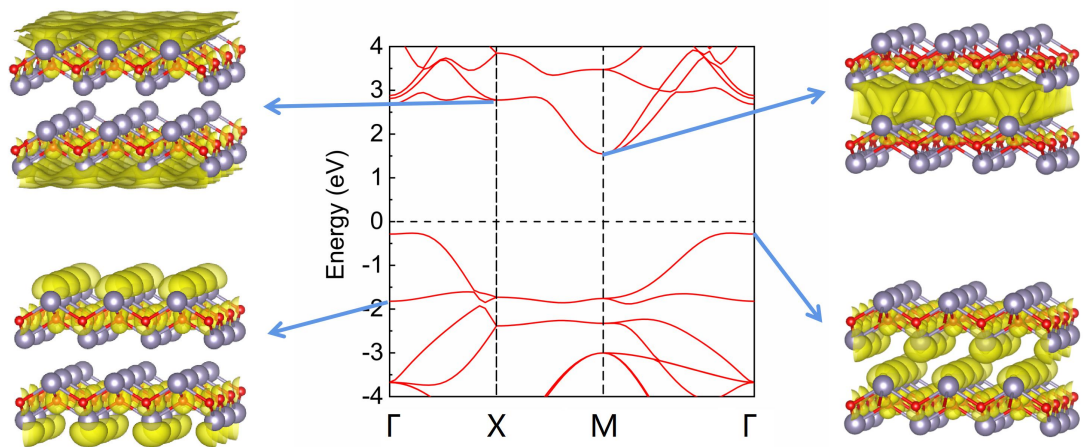


Fig. S10 Band-decomposed charge density of VBE and CBE in bilayer SnO.

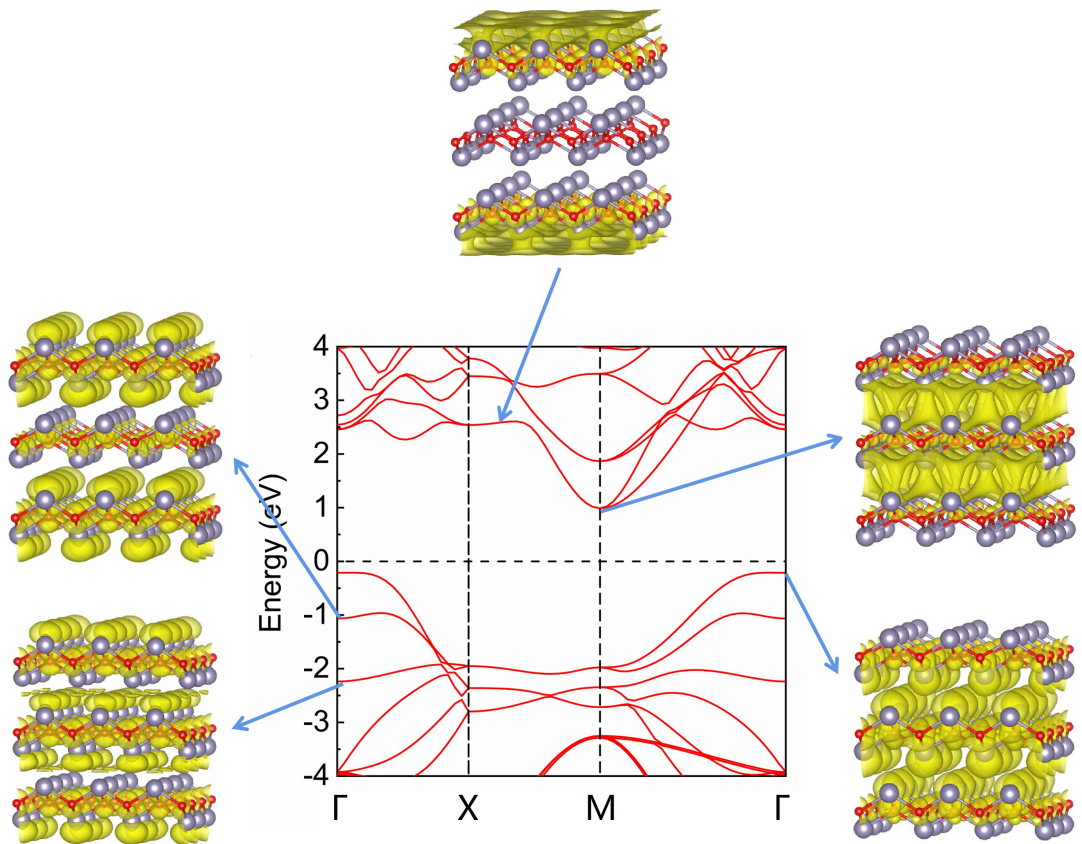


Fig. S11 Band-decomposed charge density of VBE and CBE in trilayer SnO.

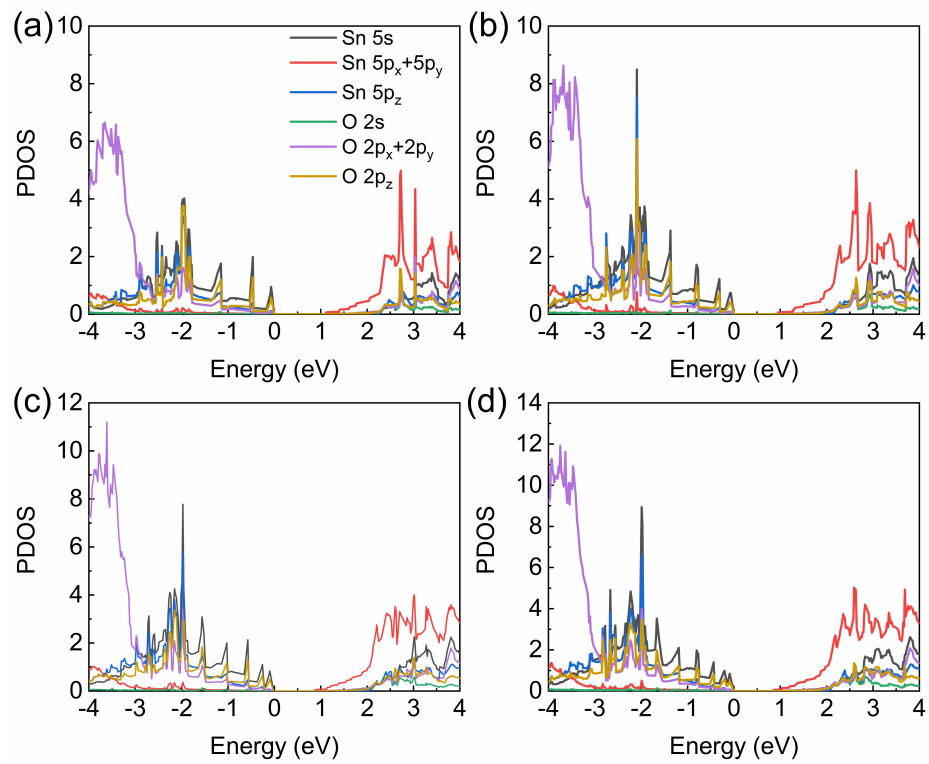


Fig. S12 Partial density of states (DOS) for (a) four-layer SnO, (b) five-layer SnO, (c) six-layer SnO, and (d) seven-layer SnO.

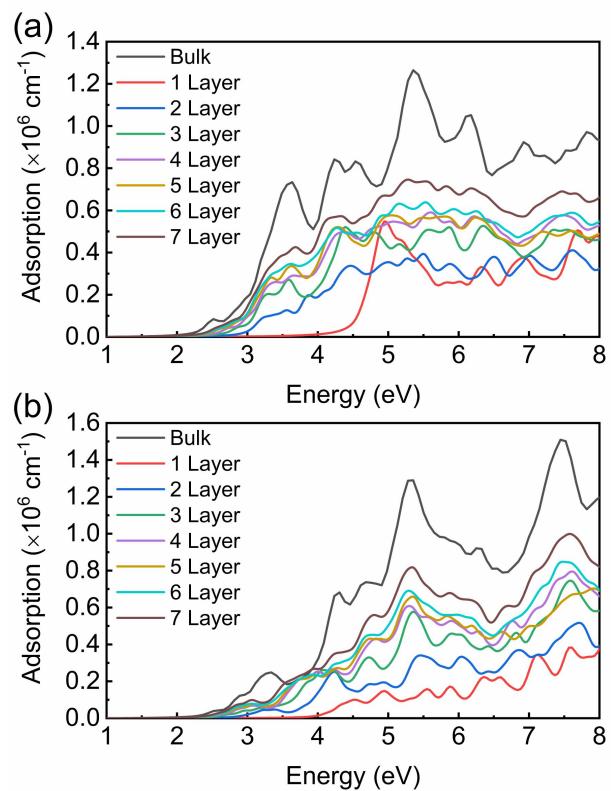


Fig. S13 Absorption spectra of layered SnO with the electric field polarized (a) parallel to the layer plane and (b) perpendicular to the layer plane.

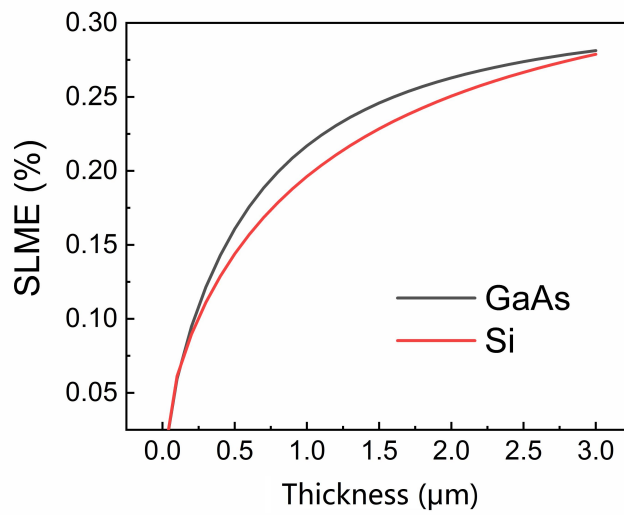


Fig. S14 Spectroscopic limited maximum efficiency of GaAs and Si with the thickness of absorbers.